Theory of photoemission from surfaces

2004 J. Phys.: Condens. Matter 16 S2539

(http://iopscience.iop.org/0953-8984/16/26/026)

INSTITUTE OF PHYSICS PUBLISHING JOURNAL OF PHYSICS: CONDENSED MATTER

J. Phys.: Condens. Matter **16** (2004) S2539–S2556 PII: S0953-8984(04)63592-2

Theory of photoemission from surfaces

J Braun and M Donath

Physikalisches Institut, Westfälische-Wilhelms Universität Münster, Wilhelm-Klemm-Straße 10, D-48149 Münster, Germany

E-mail: jbraun@uni-muenster.de

Received 16 May 2003
Published 18 June 2004
Online at stacks.iop.org/JPhysCM/16/S2539
doi:10.1088/0953-8984/16/26/026

Abstract

An improved formulation of the one-step model of photoemission from crystal surfaces is proposed which overcomes various limitations of the original theory. The model is formulated within a spin-polarized, fully relativistic framework. It applies to semi-infinite lattices with perfect lateral translational invariance and arbitrary number of atoms per unit cell. Furthermore it includes a realistic description of the solid surface to vacuum interface. Considering the result of an electronic structure calculation in the form of the electronic density functional theory potential as a given quantity, we apply the theory to magnetic thin films and multilayers and compare it with recent experimental results.

(Some figures in this article are in colour only in the electronic version)

1. Introduction

The interest in condensed materials and their surfaces has grown enormously over the last decades. In particular, the technological relevance of low-dimensional magnetic structures has triggered a lot of research activity. Nowadays miniaturization has reached the nanometre level, where surface and interface effects become dominant. Quantitative controlling of these effects, or even more a real material design, is intimately connected with a detailed understanding of the surface and interface electronic structure. Experimentally, the interesting valence band region around the Fermi energy is accessible by means of ultraviolet photoemission spectroscopy (PES) [1] and inverse photoemission (IPE) spectroscopy [2].

It is widely accepted to interpret a measured photoemission spectrum by referring to the results of band structure calculations that are based on density functional theory (DFT) and the local density approximation (LDA) [3, 4]. Provided that the electronic and geometric structure is known, some basic spectral features can be explained. To achieve a reliable interpretation of the experimental spectra, however, it is necessary to deal quantitatively with the following points. Above all, the wavevector and energy dependence of the transition-matrix elements

has to be accounted for. These dependencies are known to be important and actually cannot be neglected. They result from strong multiple-scattering processes which dominate the electron dynamics in the low-energy regime of typically 1–200 eV [5]. The transition-matrix elements also include the effects of selection rules. Last but not least, a realistic description of the surface barrier is essential for a quantitative description of surface states and resonances in simple metals but also in more complex structures like thin films and multilayers.

The most successful theoretical approach is the so-called one-step model of photoemission, as originally proposed by Pendry and co-workers [5–7]. A review of the recent developments and refinements [8] of the approach can be found in [9, 10]. The main idea of the one-step model is to describe the actual excitation process, the transport of the photoelectron to the crystal surface as well as the escape into the vacuum [11] as a single quantum-mechanically coherent process including all multiple-scattering events.

Within this model self-energy corrections, which give rise to damping processes in the quasi-particle spectrum, are properly included in both the initial and final states. This, for example, allows for transitions into evanescent bandgap states decaying exponentially into the solid. Similarly the assumption of a finite lifetime for the initial states gives us the opportunity to calculate photoemission intensities from surface states and resonances. Treating the initial and final states within the fully relativistic version of layer-KKR theory [12], it remains a simple task to design complex layered structures like thin films and multilayers within the photoemission theory. Furthermore, the very surface described by a barrier potential can be easily included into the multiple-scattering formalism as an additional layer. A realistic surface barrier which shows the correct asymptotic behaviour has been introduced, for example, by Rundgren and Malmström [13]. Therefore, one should expect that the modern theory of relativistic photoemission, in close connection with the experiment, is able to lead to a quantitative description of the surface electronic structure.

The aim of the present paper is to give an account of various new aspects concerning the appearance of surface states and resonances on simple nonmagnetic and ferromagnetic metal surfaces. We demonstrate in detail the delicate interplay between surface states and resonances which strongly depends on the geometric and magnetic surface structure. Moreover, our investigations on multilayered structures gives us the opportunity to close the conceptual gap that exists in the understanding of interface states and other surface features.

This paper is organized as follows. In sections 2 and 3 we discuss in detail the theoretical model with a special focus on surface-related intensities. Sections 4 and 5 are devoted to our experimental and theoretical results. In section 4 we start with an overview on surface states and resonances appearing on the close-packed surfaces of Cu, Ni, Co and Fe. Afterwards we switch over to the layered structure Co/Cu(100) in section 5. A summary is given in section 6.

2. One-step model of photoemission

PES and IPE are complementary spectroscopies. We concentrate on PES in the following since IPE can simply be treated analogously by taking into account geometrical factors regarding the respective experimental set-ups [14]. We start our considerations by a discussion of Pendry's formula for the photocurrent which defines the one-step model of PES [6]:

$$I^{\mathrm{PES}} \propto \mathrm{Im}\langle \epsilon_f, \boldsymbol{k}_\parallel | G_2^+ \Delta G_1^+ \Delta^\dagger G_2^- | \epsilon_f, \boldsymbol{k}_\parallel \rangle. \tag{1}$$

The expression can be derived from Fermi's golden rule for the transition probability per unit time [15]. Consequently, I^{PES} denotes the elastic part of the photocurrent. Vertex renormalizations are neglected. This excludes inelastic energy losses and corresponding quantum-mechanical interference terms [6, 15, 16]. Furthermore, the interaction of the

outgoing photoelectron with the rest system is not taken into account. This 'sudden approximation' is expected to be justified for not too small photon energies. We consider an energy-, angle- and spin-resolved photoemission experiment. The state of the photoelectron at the detector is written as $|\epsilon_f, \boldsymbol{k}_\parallel\rangle$, where $\boldsymbol{k}_\parallel$ is the component of the wavevector parallel to the surface and ϵ_f is the kinetic energy of the photoelectron. The spin state of the photoelectron is implicitly included in $|\epsilon_f, \boldsymbol{k}_\parallel\rangle$, which is understood as a four-component Dirac spinor. The advanced Green function G_2^- in equation (1) characterizes the scattering properties of the material at the final-state energy $E_2 \equiv \epsilon_f$. Via $|\Psi_f\rangle = G_2^-|\epsilon_f, \boldsymbol{k}_\parallel\rangle$ all multiple-scattering corrections are formally included. For an appropriate description of the photoemission process we must ensure the correct asymptotic behaviour of $\Psi_f(\boldsymbol{r})$ beyond the crystal surface, i.e. a single outgoing plane wave characterized by ϵ_f and $\boldsymbol{k}_\parallel$. Furthermore, the damping of the final state due to the imaginary part of the inner potential $\mathrm{i}V_{0\mathrm{i}}(E_2)$ must be taken into account. We thus construct the final state within SPLEED theory considering a single plane wave $|\epsilon_f, \boldsymbol{k}_\parallel\rangle$ advancing onto the crystal surface. Using the standard layer-KKR method [12] generalized for the relativistic case [9, 10], we first obtain the SPLEED state $U\Psi_f(\boldsymbol{r})$. The final state is then given as the time-reversed SPLEED state ($U = -\mathrm{i}\sigma_y K$ is the relativistic time inversion). Many-body effects are included phenomenologically in the SPLEED calculation by using a parametrized, weakly energy-dependent and complex inner potential $V_0(E_2) = V_{0\mathrm{r}}(E_2) + \mathrm{i}V_{0\mathrm{i}}(E_2)$ as usual [5]. This generalized inner potential takes into account inelastic corrections to the elastic photocurrent [15] as well as the actual (real) inner potential, which serves as a reference energy inside the solid with respect to the vacuum level [17]. Due to the finite imaginary part $\mathrm{i}V_{0\mathrm{i}}(E_2)$, the flux of elastically scattered electrons is permanently reduced and thus the amplitude of the high-energy wavefield $\Psi_f(\boldsymbol{r})$ can be neglected beyond a finite distance from the surface. The practical calculation starts with the Dirac Hamiltonian h_{LDA} ($\hbar = m = e = 1, c = 137.036$) which one has to consider in the framework of relativistic DFT [18, 19]:

$$h_{\mathrm{LDA}}(\boldsymbol{r}) = -\mathrm{i}c\boldsymbol{\alpha}\boldsymbol{\nabla} + \beta c^2 - c^2 + V_{\mathrm{LDA}}(r) + \beta\boldsymbol{\sigma}\boldsymbol{B}_{\mathrm{LDA}}(r). \tag{2}$$

$V_{\mathrm{LDA}}(r)$ denotes the (effective) spin-independent potential and $\boldsymbol{B}_{\mathrm{LDA}}(r)$ is the (effective) magnetic field. They are given as [20]

$$V_{\mathrm{LDA}}(r) = \tfrac{1}{2}(V_{\mathrm{LDA}}^{\uparrow}(r) + V_{\mathrm{LDA}}^{\downarrow}(r)), \qquad \boldsymbol{B}_{\mathrm{LDA}}(r) = \tfrac{1}{2}(V_{\mathrm{LDA}}^{\uparrow}(r) - V_{\mathrm{LDA}}^{\downarrow}(r))\boldsymbol{b}. \tag{3}$$

The constant unit vector $\boldsymbol{b}$ determines the spatial direction of the (uniform) magnetization as well as the spin quantization axis. β denotes the usual 4×4 Dirac matrix with the nonzero diagonal elements $\beta_{11} = \beta_{22} = 1$ and $\beta_{33} = \beta_{44} = -1$, and the vector $\boldsymbol{\alpha}$ is given by its components $\alpha_k = \sigma_x \otimes \sigma_k$ ($k = x, y, z$) in terms of the 2×2 Pauli matrices σ_k. Solutions of the corresponding Dirac equation may be found by use of the phase-functional ansatz of Calogero [21] generalized to the relativistic case [22–25]. From this solution it is easy to define the atomic scattering matrix Γ for a single ion-core potential together with the wavefunctions for the initial and final state. The atomic scattering matrix Γ together with the crystal geometry determines the scattering matrix M for a single layer. By means of layer-doubling techniques the so-called bulk-reflection matrix can be calculated, which gives the scattering properties of a semi-infinite stack of layers. Finally, applying the SPLEED theory [12] we are able to derive the final state for the semi-infinite crystal.

Δ in equation (1) is the dipole operator in the electric dipole approximation which is well justified in the visible and ultraviolet spectral range. It mediates the coupling of the high-energy final state with the low-energy initial states. In a fully relativistic theory the dipole interaction of an electron with the electromagnetic field is given by the dipole operator $\Delta = -\boldsymbol{\alpha}\boldsymbol{A}_0$, where $\boldsymbol{A}_0$ is the spatially constant vector potential inside the crystal. In a matrix element

$\langle\Psi_f|\Delta|\Psi_i\rangle$ between eigenspinors $|\Psi_f\rangle$ and $|\Psi_i\rangle$ of the Dirac Hamiltonian with energies E_f and E_i, respectively, Δ follows as

$$\Delta = E_{fi}\left(\boldsymbol{A}_0\boldsymbol{\nabla} + \frac{\mathrm{i}\omega}{c}\boldsymbol{\alpha}\boldsymbol{A}_0\right)V_{\mathrm{LDA}} + E_{fi}(\boldsymbol{A}_0\boldsymbol{\nabla})\beta\boldsymbol{\sigma}\boldsymbol{B}_{\mathrm{LDA}} + E_{fi}\frac{\omega}{c}\beta\boldsymbol{A}_0\times\boldsymbol{\sigma}\boldsymbol{B}_{\mathrm{LDA}}, \tag{4}$$

with $E_{fi} = -2\mathrm{i}c/[(E_f + c^2)^2 - (E_i + c^2)^2]$. The expression is derived by making use of commutator and anticommutator rules analogously to the nonrelativistic case in [26].

The 'low-energy' propagator G_1^+ in equation (1), i.e. the one-electron retarded Green function for the initial state in the operator representation, yields the 'raw spectrum'. It is directly related to the 'bare' photocurrent and thereby represents the central physical quantity within the one-step model. $G_1^+ \equiv G_1^+(E_i)$ is to be evaluated at the initial-state energy $E_i \equiv \epsilon_f - \omega - \mu_0$, where ω is the photon energy (μ_0 stands for the chemical potential). In the relativistic case G_1^+ is described by a 4×4 Green matrix which has to be obtained for a semi-infinite stack of layers. According to Pendry [6] the calculation of G_1^+, and, as a consequence the calculation of the photocurrent, can be divided into four different steps. The first contribution, the so-called 'atomic contribution', results from the replacement of G_1^+ in equation (1) by $G_{1,a}^+$. This quantity is defined by the following equation:

$$[E_i + \mu_0 - h_{\mathrm{LDA}}(\boldsymbol{r})]G_{1,a}^+(\boldsymbol{r},\boldsymbol{r}',E_i) = -\delta(\boldsymbol{r}-\boldsymbol{r}'). \tag{5}$$

Finally, the atomic contribution is built up by a product between the matrix $\mathcal{Z}^1$ and the multiple scattering coefficients $A_{jn\kappa\mu}$ of the final state. Here n denote the nth cell of the jth layer and κ, μ are the conventional relativistic indices. It follows that

$$I^a(\epsilon_f,\boldsymbol{k}_\parallel) \propto \mathrm{Im}\sum_{jn}\sum_{\kappa\mu\kappa'\mu'} A_{jn\kappa\mu}\mathcal{Z}^1_{jn\kappa\mu\kappa'\mu'}A^*_{jn\kappa'\mu'}. \tag{6}$$

For an explicit calculation $\mathcal{Z}^1$ must be separated into angular matrix elements and radial double matrix elements. A detailed description of the matrix $\mathcal{Z}^1$ and of the multiple scattering coefficients $A_{jn\kappa\mu}$ is given in [9, 10]. The intra(inter)-layer contributions to the photocurrent describe the multiple scattering corrections of the initial state G_1^+ between and within the layers of the single crystal. They can be written in a similar form:

$$I^m(\epsilon_f,\boldsymbol{k}_\parallel) \propto \mathrm{Im}\sum_{jn}\sum_{\kappa\mu\kappa'\mu'} A_{jn\kappa\mu}\mathcal{Z}^2_{jn\kappa\mu\kappa'\mu'}C^{B,G}_{jn\kappa'\mu'}. \tag{7}$$

Here C^B and C^G denote the multiple scattering coefficients of the initial state within a layer and between different layers. Analogously the matrix $\mathcal{Z}^2$ can be separated into angular and radial parts. The difference to the atomic contribution is that the radial part of the matrix $\mathcal{Z}^2$ consists of radial single matrix elements instead of radial double integrals. For a detailed description of the matrix $\mathcal{Z}^2$ and of the multiple scattering coefficients C^B and C^G the reader is again referred to [9, 10].

Within the last contribution to the photocurrent one takes care of the surface of the semi-infinite crystal. In particular, it follows for the surface part of the photocurrent:

$$I^s(\epsilon_f,\boldsymbol{k}_\parallel) \propto \mathrm{Im}\int \mathrm{d}\boldsymbol{r}\,\Psi_f^{*s}(\boldsymbol{r})\triangle\Psi_i^s(\boldsymbol{r}), \tag{8}$$

with

$$\Psi_i^s(\boldsymbol{r}) = \int \mathrm{d}\boldsymbol{r}'\,G_s^+(\boldsymbol{r},\boldsymbol{r}')\triangle^*\Psi_f^s(\boldsymbol{r}'). \tag{9}$$

In the case of a z-dependent barrier potential $V_B = V_B(z)$, the initial- and final-state wavefields have to be calculated numerically in the surface region, as has been shown by Grass *et al* [27].

Both wavefields $\Psi_i^s(\boldsymbol{r})$ and $\Psi_f^s(\boldsymbol{r})$ can be decomposed into z-dependent and corresponding parallel components:

$$\Psi_i^s(\boldsymbol{r}) = \sum_{\boldsymbol{g}} \phi_{\boldsymbol{g}}(z) \mathrm{e}^{\mathrm{i}\boldsymbol{k}_{i\boldsymbol{g}_\parallel}(\boldsymbol{r}-\boldsymbol{c})_\parallel}, \tag{10}$$

$$\Psi_f^s(\boldsymbol{r}) = \sum_{\boldsymbol{g}} \chi_{\boldsymbol{g}}(z) \mathrm{e}^{\mathrm{i}\boldsymbol{k}_{f\boldsymbol{g}_\parallel}(\boldsymbol{r}-\boldsymbol{c})_\parallel}, \tag{11}$$

with the regular solutions of the Schrödinger equation $\phi_{\boldsymbol{g}}$ and $\chi_{\boldsymbol{g}}$ to the reciprocal lattice vector $\boldsymbol{g}$ for $V_B(z)$ in the range $-\infty < z < c_z$. The value c_z defines the point where the surface potential goes smoothly into the inner potential of the bulk crystal.

Final evaluation of the surface contribution gives

$$I^s(\epsilon_f, \boldsymbol{k}_\parallel) \propto \mathrm{Im} \sum_{\boldsymbol{g}} \mathrm{e}^{\mathrm{i}\boldsymbol{q}_\parallel \cdot \boldsymbol{c}_\parallel} A_z \int_{-\infty}^{c_z} \phi_{\boldsymbol{g}} V_B' \chi_{\boldsymbol{g}} \mathrm{e}^{\mathrm{i}q_z z} \, \mathrm{d}z, \tag{12}$$

where A_z is the z component of the amplitude $\boldsymbol{A}_0$ and $\boldsymbol{q}$ is the wavevector of the photon field. For a step barrier $V_B(z) = V_{\mathrm{or}}\Theta(z - c_{1z})$, where Θ is the unit step function, Pendry's result [6] will be reproduced. V_{or} denotes the constant inner potential of the bulk crystal.

The spin-dependent Rundgren–Malmström barrier [13] connects the asymptotic regime $z < z_A$ to the bulk muffin-tin zero V_{or} by a third-order polynomial in z, spanning the range $z_A < z < z_E$. The zero of the z scale lies in the uppermost layer of atoms. For the real parts of $V_B^{\uparrow(\downarrow)}(z)$ we have

$$V_B^{\uparrow(\downarrow)}(z) = \begin{cases} \frac{1}{4}(z - z_I^{\uparrow(\downarrow)})^{-1} & z < z_A^{\uparrow(\downarrow)} < z_I^{\uparrow(\downarrow)}, \\ s_0^{\uparrow(\downarrow)} + & \\ s_1^{\uparrow(\downarrow)}(z - z_A^{\uparrow(\downarrow)}) + & \\ s_2^{\uparrow(\downarrow)}(z - z_A^{\uparrow(\downarrow)})^2 + & \\ s_3^{\uparrow(\downarrow)}(z - z_A^{\uparrow(\downarrow)})^3 & z_A^{\uparrow(\downarrow)} < z < z_E^{\uparrow(\downarrow)}, \\ V_{\mathrm{or}} & z > z_E^{\uparrow(\downarrow)}. \end{cases} \tag{13}$$

The imaginary parts of the barrier potential have been set to zero, avoiding the introduction of additional parameters. $z_I^{\uparrow(\downarrow)}$ denote the position of the classical spin-dependent image planes. The polynomial coefficients $s_0^{\uparrow(\downarrow)}$, $s_1^{\uparrow(\downarrow)}$, $s_2^{\uparrow(\downarrow)}$, $s_3^{\uparrow(\downarrow)}$ are fixed through the requirement of continuity and differentiability for $V_B^{\uparrow(\downarrow)}(z)$.

3. Surface state analysis by resonance criterion

From the theoretical point of view a quantitative spectroscopic approach is needed which explains the origin of the various intensity features, thereby distinguishing between surface states and surface resonances. In the framework of multiple scattering theory, general conditions for the occurrence of surface structures have been developed [28, 29]. They considered a wavefield ϕ, multiply scattered between the topmost layer of the semi-infinite bulk crystal and the surface barrier potential V. The surface barrier connects the inner potential of the bulk crystal with the vacuum level respecting the long range image-potential behaviour, which is well known from classical electrodynamics. Having calculated the reflection matrices of the bulk crystal $\boldsymbol{R}_b$ and of the barrier potential $\boldsymbol{R}_v$, the following condition for the existence of a surface state can be obtained [28, 29]:

$$|\det(\mathbb{1} - \boldsymbol{R}_b \boldsymbol{R}_v)| = 0. \tag{14}$$

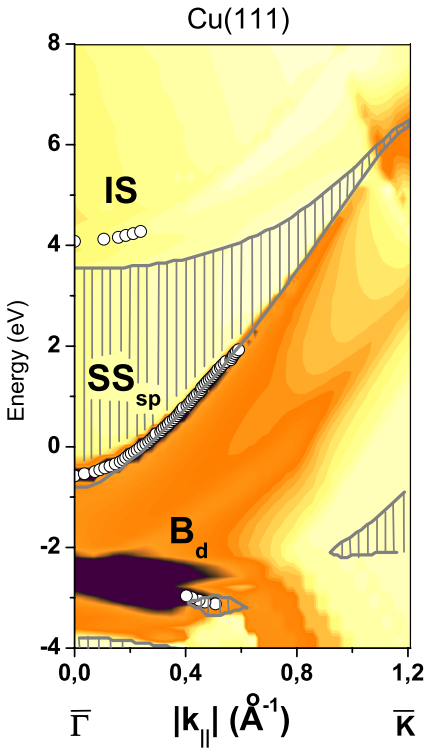

Figure 1. Contour plot for calculated (I)PE spectral densities of Cu(111) along $\bar{\Gamma}\bar{\mathrm{K}}$ for a photon energy of $\hbar\omega = 9.4$ eV. Values of high spectral density are shown by dark regions. Shaded areas represent gaps in the projected bulk band structure. IS denotes the $n = 1$ image-potential state. $\mathrm{SS_{sp}}$ denotes a sp-like Shockley state. The d-like bulk emission is indicated by B_{d}. The dispersion behaviour of the surface features, derived by analysing the resonance criterion, is shown by open circles.

The appearance of a surface resonance is simply indicated by a minimum of $|\det(\mathbb{1} - \boldsymbol{R}_b \boldsymbol{R}_v)|$. With this condition a strategy for the classification of surface structures is given. One has to calculate the photocurrent for a given symmetry direction in the surface Brillouin zone together with the resonance condition, which is shown in equation (14). The results of our analysis will be seen in figures 1 and 4–6. The projected bulk band structures (shaded areas) result from potentials calculated by use of the self-consistent tight-binding linear muffin-tin (TB-LMTO) method [30]. Together with a surface barrier these potentials represent the electronic structure underlying our relativistic one-step calculations of the (I)PE spectral densities (colour scaled contour plots). Lifetime effects in the final and initial states have been included in our analysis in a phenomenological way using a parametrized complex inner potential $V_{\mathrm{o}}(E) = V_{\mathrm{or}}(E) + \mathrm{i}V_{\mathrm{oi}}(E)$. Here, the real part serves as a reference energy inside the crystal with respect to the vacuum level. For the final and initial states constant imaginary parts $\mathrm{i}V_{\mathrm{oi}}(E_2) = 2.0$ and $\mathrm{i}V_{\mathrm{oi}}(E_1) = 0.01$ eV have been chosen. A realistic description of the surface potential is given through a spin-dependent Rundgren–Malmström barrier $V^{\uparrow\downarrow}(z)$ [13], which connects the asymptotic regime $\sim 1/z$ to the bulk muffin-tin zero V_{or} by a third-order polynomial in z. In order to exclude artificial parametrizations for the surface barrier we followed the procedure described in detail in [31]. The open circles in figures 1 and 4–6 define the $E(\boldsymbol{k}_{\parallel})$ values which fulfil the resonance condition.

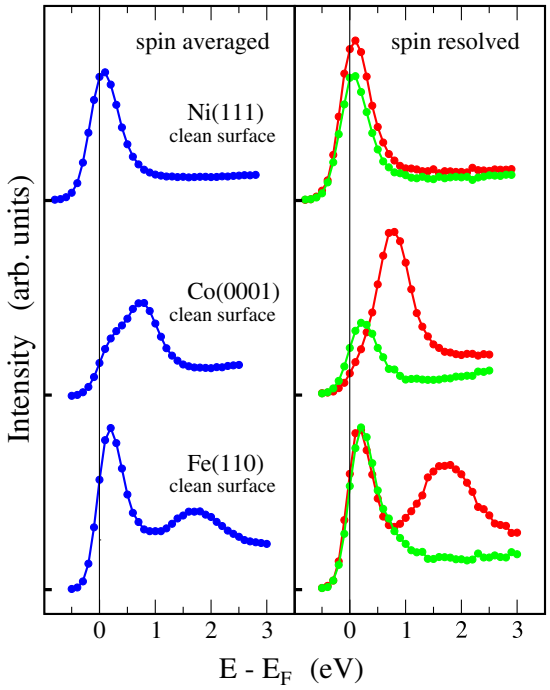

Figure 2. Spin-averaged (left-hand side) and spin-resolved (right-hand side) IPE spectra of the clean surfaces of Ni(111), Co(0001) and Fe(110) at $\bar{\Gamma}$ ($\hbar\omega = 9.4$ eV).

4. Electronic structure of simple metal surfaces

In simple nonmagnetic metals electronic surface states are well understood as far as binding energies and $E(\boldsymbol{k}_\parallel)$ dispersions are concerned [32]. Today, only lifetime effects are still a research topic. Switching over from nonmagnetic simple sp-band metals like Cu, Ag or Au to the 3d ferromagnets, the situation becomes more complicated and even unclear [33]. This observation is not at all astonishing simply because of the appearance of magnetism. In other words, we have to deal with narrow spin-split d bands in the vicinity of the Fermi level in addition to strongly dispersing sp-like bands. As prototypical cases with quite similar bandgap situations, let us focus on the close-packed surfaces of fcc Cu(111), Ni(111), hcp Co(0001) and bcc Fe(110).

We start our considerations with Cu(111). In this case only one sp-like surface state is expected and experimentally confirmed at the bottom of the $L_{2'}$–L_1 sp bandgap. A contour plot for calculated (I)PE spectral densities of Cu(111) along $\bar{\Gamma}\bar{\mathrm{K}}$ is shown for a photon energy of $\hbar\omega = 9.4$ eV in figure 1. Dark regions represent high values of spectral density, whereas the yellow pattern indicate nearly zero I(PE) intensity. The energy gaps in the projected bulk band structure have been marked by grey shaded areas. IS and $\mathrm{SS_{sp}}$ denote the $n = 1$ image-potential state and the sp-like Shockley state, respectively. B_d indicates d-like bulk emission. The calculated dispersion behaviour of all surface features, which fulfil the resonance condition, is visualized by open circles.

Based on the understanding of surface states on non-ferromagnetic Cu(111), we move on to ferromagnetic Ni(111), Co(0001) and Fe(110). Experimental IPE results for normal electron incidence and a photon takeoff angle of about 35° with respect to the surface normal

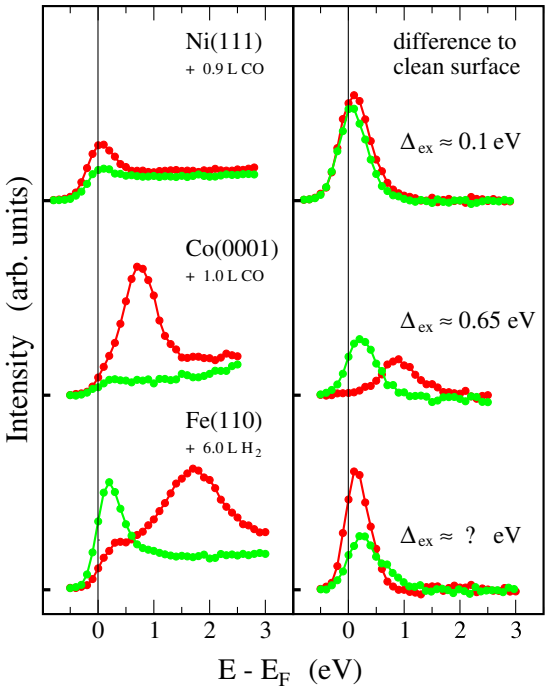

Figure 3. Spin-resolved (left-hand side) IPE spectra of the contaminated surfaces of Ni(111), Co(0001) and Fe(110) at $\bar{\Gamma}$ ($\hbar\omega = 9.4$ eV). Corresponding difference spectra to the clean surfaces are shown on the right-hand side.

are presented in figures 2 and 3. Figure 2 shows spin-averaged (left-hand panel) and spin-resolved (right-hand panel) data for the clean surfaces. The spin-averaged data (blue (black)) are the sum of the minority (red (dark grey)) and majority results (green (light grey)), divided by a factor of two. From the spectra it is not possible to distinguish between bulk and surface contributions. Therefore, the surfaces were exposed to CO or H_2 gas. For details about the choice of the adsorbate and amount of the exposure ($1\ \mathrm{L} = 1.33 \times 10^{-4}$ Pa s), the reader is referred to the particular case studies [31, 34, 35]. The adsorbates were observed to quench the surface contributions. Figure 3 displays the spin-resolved IPE data of the contaminated surfaces (left-hand side intensities) and the difference spectra (right-hand side). With the assumption that the difference spectra represent the surface contributions, Ni(111) shows a partially occupied surface state right at the Fermi level with an exchange splitting of about 0.1 eV, Co(0001) exhibits an unoccupied surface state with about 0.65 eV exchange splitting, while the situation for Fe(110) with asymmetric spectral features and almost no spin splitting seems unclear. The bulk contributions, derived from the left part of figure 3, show nicely the d bands shifting to higher energies relative to E_F from Ni to Co to Fe. While Ni and Co are strong ferromagnets with only minority d states empty, Fe is called a weak ferromagnet with empty majority d states as well (see the majority peak just above the Fermi level). The d state intensity in the Ni spectrum is low because no direct transition into d states is possible for the chosen point in $\boldsymbol{k}$ space. In the following, we will discuss the three ferromagnetic surfaces in detail, first from the experimental and then from the theoretical point of view.

From a literature study of surface states on Ni(111), it is legitimate to assume both the existence or nonexistence of two spin-split surface states at $\bar{\Gamma}$. Based on spin-averaged PE data,

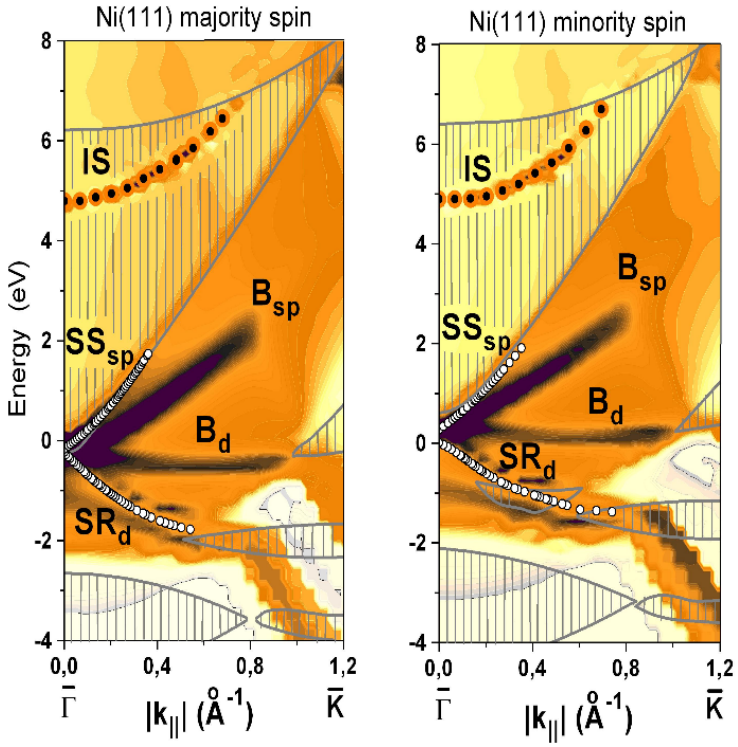

Figure 4. Calculated contour plots for majority (left panel) and minority (right panel) (I)PE spectral densities of Ni(111) along $\bar{\Gamma}\bar{K}$ for a photon energy of $\hbar\omega = 9.4$ eV. Values of high spectral density are shown by dark regions. Shaded areas represent gaps in the projected bulk band structure. IS denotes the $n = 1$ image-potential state. SS_{sp} denotes a sp-like Shockley state. Features denoted by SR_d were identified as d-derived surface resonances. The sp- and d-like bulk emissions are indicated by B_{sp} and B_d, respectively. The open circles represent the $E(\boldsymbol{k}_{\parallel})$ values which fulfil the resonance condition for crystal-induced surface states/resonances.

one [36, 37] or two [38] occupied surface state(s) were reported with a pronounced dispersion behaviour around $\bar{\Gamma}$. On the other hand, an exchange-split surface state, partially occupied in its majority component, was detected by spin-resolved IPE, as shown in figures 2 and 3 [34]. The prominent spectral feature just above the Fermi level appears in both partial spin spectra. Since at $T = 0$ no empty majority d states are available in Ni, one may conclude that the spin-up emission at E_F does not originate from direct transitions into d states. To clarify the origin of this feature, its sensitivity to surface contamination was tested. It is clearly visible that the small remaining feature close to E_F on the contaminated surface exhibits a high spin asymmetry and is, therefore, interpreted as indirect transitions into minority d states, which are known to be not very surface sensitive. The corresponding difference spectra support an interpretation in terms of an exchange-split surface state which is cut off by the Fermi function at least for the majority part.

A similar bandgap situation is found for Co(0001). Figure 2 (middle part) shows spin-averaged and spin-resolved IPE spectra for normal electron incidence [31]. The spin-averaged spectrum reveals an asymmetric intensity distribution with at least two contributions, which can be separated by the use of spin resolution. The minority peak at 0.75 eV obviously stems from a transition into a bulk d band, which disperses downward in the Brillouin zone

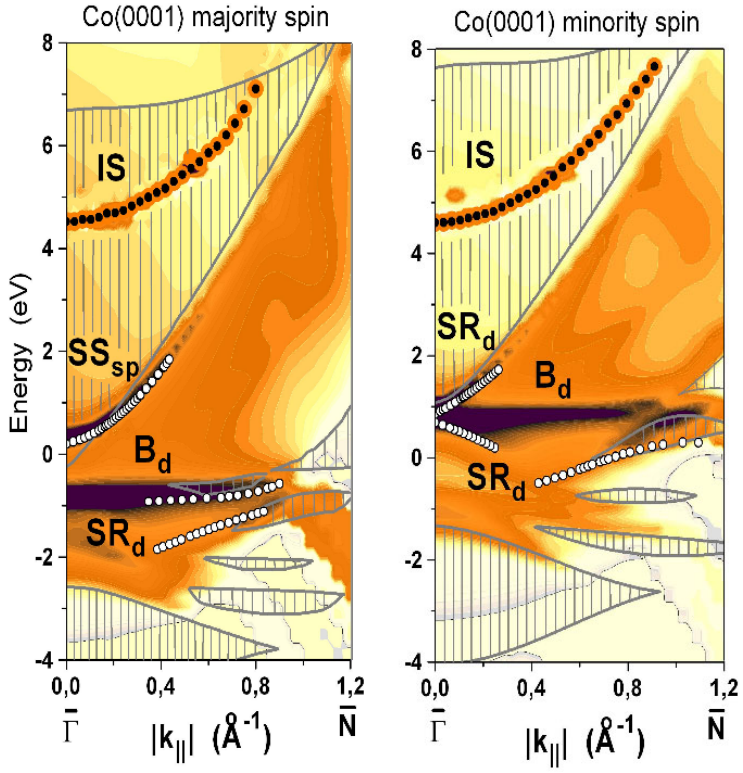

Figure 5. Contour plots for majority (left panel) and minority (right panel) (I)PE spectral densities of Co(0001) along $\bar{\Gamma}\bar{N}$. For details of the notation see figure 4.

along Δ from about 1.0 eV at Γ to 0.7 eV at A. However, the peak at 0.25 eV above E_F has majority character, even though no majority bulk d bands are expected to appear above E_F. Therefore, one may think about a crystal-induced surface state, located in the projected bulk band gap at $\bar{\Gamma}$. To gain more information about possible surface features, we refer to the data of the adsorbate experiment in figure 3. The surface sensitivity of the majority-spin state at 0.25 eV above E_F is clearly demonstrated by the complete quenching of the peak in the spectrum of the contaminated surface. The minority peak is affected by CO to a much smaller degree, as is expected for a bulk state transition. However, the asymmetric reduction of the peak intensity points to the presence of a transition into another minority state which is energetically separated from the d-band transition but cannot be resolved due to lifetime broadening and/or to the limited resolution of our experiment. This state clearly shows up in the difference spectra presented in the middle part of figure 3 (right side). In general, difference spectra have to be interpreted with care. They contain surface-sensitive contributions of the clean surface as well as additional adsorbate-induced modifications of the electronic structure. Nevertheless, the adsorbate-induced empty $2\pi^*$ state of CO chemisorbed on transition metals is known to be located at energies higher than 2 eV above E_F [39], i.e. well above the energy range under consideration here. Therefore, we assume that the minority structure at 0.9 eV above E_F in the difference spectrum represents mainly the surface-state emission. Therefore, it is strong evidence that Co(0001) exhibits an unoccupied surface state with a surprisingly large exchange splitting compared with the splitting of the p-derived lower bandgap boundary [31].

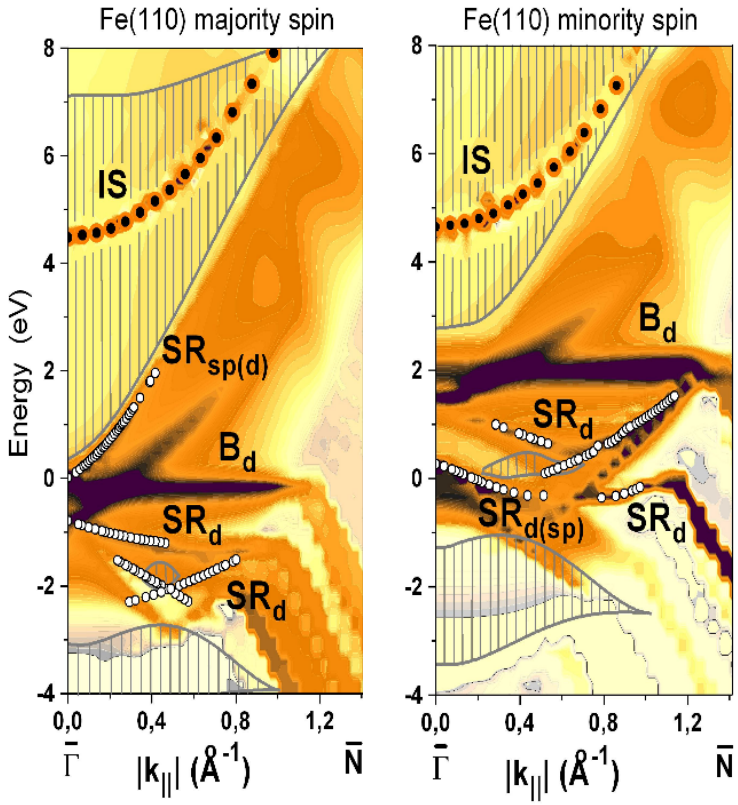

Figure 6. Contour plots for majority (left panel) and minority (right panel) (I)PE spectral densities of Fe(110) along $\bar{\Gamma}\bar{N}$. $SR_{sp(d)}$ and $SR_{d(sp)}$ denote surface resonances with mixed symmetry character. For details of the notation, see figure 4.

In addition, IPE measurements with different photon takeoff angle reveal that the two spin components exhibit a different photon emission characteristic, indicating somewhat different symmetry for the minority and majority transitions. Furthermore, this result of an unoccupied surface state seems to be in conflict with a former spin-averaged PE experiment [40, 41], in which an occupied surface state was already measured at about 0.3 eV below E_F.

For Fe(110), the experiments reported so far are also not conclusive with respect to surface states. One spin-averaged PE study reports on a surface state located at 0.15 eV below E_F at $\bar{\Gamma}$ [42]. In another PE investigation with spin resolution, a minority surface feature was observed at 0.5 eV below E_F at 0.5 $\bar{\Gamma}\bar{H}$ [43]. Recent work reports on spin-split resonance-like features on Fe(110) [35, 44]. In the lower parts of figures 2 and 3 we present spin-averaged and spin-resolved IPE data for the clean and hydrogen-exposed Fe(110) surface [35]. The spin-averaged spectrum reveals at least two peaks. The spin resolution allows us to identify three spectral features in the corresponding spectra (figure 2 right side). Two peaks are locatable just above the Fermi energy: a minority and a majority spectral feature. The third one is of pure minority character and is easily explained as minority d-band emission. The features close to the Fermi level appear at slightly different energies for spin-up and spin-down electrons. Their origin is investigated by exposing the surface to hydrogen. CO turned out to be not a suitable test adsorbate because, in contrast to experiments with the Ni(111) [34] and Co(0001)[31] surfaces, it quenches the bulk d-band emission as well. 6 L of H_2 do not affect the minority

bulk emission but influence the features close to E_F in an elucidating way. It is clearly seen from figure 3 (left side) that the minority peak disappears completely while the majority peak is only partially quenched. The remaining majority feature is attributed to majority bulk d bands. The corresponding difference spectra, representing the surface-sensitive features, are displayed in the lower part of figure 3 (right side). They reveal a minority structure and a smaller majority peak with a peculiar asymmetric lineshape. The majority peak maximum appears at a slightly higher energy than the maximum of the minority peak. This observation is in contrast to the expectation of a simple spin-split surface state with the minority-spin part higher in energy than the majority part.

This experimental overview of the close-packed surfaces of 3d ferromagnets makes it very clear that the appearance of surface-related electronic states is much more complex here than on simple metal surfaces like Cu. Owing to the various d bands which appear in (magnetic) 3d metals around the Fermi level, a variety of surface states and other surface-related features should be observable. Strong evidence for this hypothesis is given by our spectral analysis that will be presented in the following.

We will start our discussion with Ni(111) because it is the case most similar to Cu(111). The Shockley-inverted gap spanning from $L_{2'}$ to L_1 is, at variance with Cu(111), traversed by an exchange-split d band which, however, has a different symmetry than the p-derived state at the bottom of the gap at $\bar{\Gamma}$. The total gap region appearing in the projected bulk band structure is indicated by perpendicular lines in figure 4. We find the $n = 1$ member of the image-potential state series (IS) inside, bulk emission from sp and d bands ($B_{sp(d)}$) outside the gap, and surface-related features SS_{sp} and SR_d. The influence of d bands on the surface electronic properties is significantly enhanced compared with Cu because they are much closer in energy to the Fermi level and therefore touching the gap at $\bar{\Gamma}$. Nevertheless a sp-like surface state SS_{sp}, similar to the Cu(111) case, with positive dispersion is found in both spin channels. The exchange splitting, determined by the lower sp-gap boundary, amounts to 350 meV, in contrast to spin-resolved IPE results yielding about 100 meV. An explanation for this discrepancy can be found in the well-known result that DFT(LDA) calculations overestimate the exchange splitting in ferromagnetic Ni by about a factor of two. In addition, the exchange splitting at $\bar{\Gamma}$ is not directly accessible to the experiment because the majority spin state is found slightly below E_F. Our calculation reveals an additional surface feature, a d-like spin-split surface resonance with a negative dispersion but zero intensity at $\bar{\Gamma}$. The pronounced decrease in intensity is due to the fact that spectral weight is shifted from the resonance to the bulk d band while approaching $\bar{\Gamma}$. The sp-like surface state, of course, survives at $\bar{\Gamma}$ and is detectable also for normal electron (incidence) emission in (I)PE. Details of the experiment, i.e. finite energy and angular resolution as well as the precision of the orientation of the sample mirror plane with respect to the impinging or emitted electrons, will decide about the appearance of one or two surface-sensitive features in the spectroscopic data, even in nominally 'normal' (incidence) emission geometry [45].

The situation for Co(0001) is, as expected, even more complicated. The contour plot for the majority (I)PE spectral density shown in the left panel of figure 5 reveals three surface-sensitive features, a sp-like surface state SS_{sp} with positive dispersion and two d-like resonances SR_d. The resonances, which are visible only for specific $|k_\parallel|$ values, disperse in the neighbourhood of minor bulk bandgaps. Also shown is IS and the bulk emission B_d from a Co 3d band. This case is comparable to Cu(111) because no resonance-like structures appear around $\bar{\Gamma}$ in the vicinity of the main volume gap. The influence of d bands is much stronger in the minority case. In addition to the well-known features IS and B_d, three d-like surface resonances exist but no sp-like surface state. In a reference calculation without d states, only one surface feature appears near $\bar{\Gamma}$, shifted to lower energy by about 0.4 eV compared with SR_d and with

positive dispersion like the majority SS_{sp}. This result attributes the unexpected large exchange splitting (≈0.7 eV) and the spin-dependent polarization [31] to the different influence of the d bands in the majority and minority spin systems. Therefore, the two surface peaks, which were identified above E_F on Co(0001), cannot be interpreted as 'spin partners' any more. The detailed symmetry analysis reveals a pure sp-like surface state in the majority channel at $\bar{\Gamma}$. In the minority channel a masked sp-like surface state exists, which is forced by the intimate neighbourhood of d states to behave as a d-like surface resonance. In other words, the d contribution in this surface feature is dominant, but nonnegligible sp-like contributions are present. The other crystal-induced surface structures show a pure d character when analysing their symmetry behaviour. Similar to Ni(111), only one surface feature exists in the minority channel at $\bar{\Gamma}$ because the spectral weight is zero for the other resonance at $\boldsymbol{k}_\parallel = 0$. In contrast to former experimental work [40, 41], no surface-sensitive features are found below E_F [45].

Comparing the surface electronic properties of Ni(111) and Co(0001), a tendency against sp-like surface states is clearly observable. For Fe(110) the 'contest' between these surface structures has been decided in favour of resonances. Figure 6 shows exclusively surface resonances in addition to IS and B_d but no single surface state on Fe(110). Similar to Co(0001), some resonances of pure d-character, denoted by SR_d, disperse along smaller gaps, but they do not approach $\boldsymbol{k}_\parallel = 0$. Three candidates appear at $\bar{\Gamma}$, a pure d-like resonance with majority spin character and two features denoted as $SR_{sp(d)}$ and $SR_{d(sp)}$. The resonance SR_d should appear in the majority PE channel ≈0.8 eV below E_F at $\boldsymbol{k}_\parallel = 0$, but one should realize that its intensity decreases strongly when approaching $\bar{\Gamma}$. In agreement with our analysis, the spin-resolved IPE experiments shown in figures 2 and 3 reveal two surface-sensitive features for normal electron incidence, which are located in energy just above E_F. According to our calculation, the majority type resonance $SR_{sp(d)}$ exhibits a positive dispersion, which is caused by the gap boundary. For the minority resonance $SR_{d(sp)}$ a less pronounced dispersion in the opposite direction is obtained. The peculiar dispersion behaviour of this resonance is easily understood in terms of the electronic properties of ferromagnetic Fe in the vicinity of E_F. At first, one may notice that the symmetry character of the lower gap boundary at $\bar{\Gamma}$ is different in the two spin channels. This is due to the different band order of sp and d bands along ΓN. In the majority channel $SR_{sp(d)}$ is located in energy above the d bands and therefore disperses from E_F at $\bar{\Gamma}$ to higher energies, unhindered by d bands. To learn more about the symmetry character of $SR_{sp(d)}$ we repeated the spectroscopic calculations without considering d states. From this procedure the resonance was found to be still alive, but shifted to lower energies by about 0.2 eV. This result confirms the 'd-caused' trend against sp-like surface states, which was discussed before. The majority Shockley state from Co(0001) is turned into a resonance on Fe(110) by an admixture of d-band character. The same type of analysis applied to the minority emission reveals another interesting detail of the surface electronic structure of Fe(110). Suppressing artificially the influence of d states keeps the feature $SR_{d(sp)}$ alive, but with a switch from negative to positive dispersion. This means, the resonance character forced by the d states is removed and the resonance mutates into a surface state that disperses in an ordinary sp-type symmetry gap. The gap itself opens through the disappearance of d bands [45].

5. Extension to quantum-well states

In the previous chapter we discussed in detail the surface electronic structure of the close-packed surfaces of Cu, Ni, Co and Fe. An intimate relationship between crystal-induced surface states and surface resonances was found. In detail, sp-like surface states on Cu and

Ni tend to transform into d-like resonances on Co and Fe. This process is correlated with the growing number of d states around E_F. Moving from simple metal surfaces to more complicated systems like multilayers new features in the electronic structure appear, the so-called quantum-well (QW) states. Such states, which are observable in addition to surface states and resonances, are commonly described within the phase accumulation model (PAM) [46, 47]. A typical example for a magnetic multilayer is Co/Cu(100). This nanostructure has both significance in fundamental research and relevance in technological applications. For small or large film thicknesses of Co, the surface electronic structure of Co/Cu(100) should be comparable to that of the clean surfaces of fcc Cu(100) and fcc Co(100). This is a further advantage, which helps one to study the development of QW states as a function of layer thickness.

Experimentally, we investigated the unoccupied QW states of Co/Cu(100) at room temperature for Co film thicknesses up to 12 monolayers (ML) [48]. The results of our IPE experiment have been collected in figure 7. As a function of the film thickness we present the spin-averaged spectra in the left panel (figure 7(a)). The spin-resolved data are shown in the right panel (figure 7(b)). All spectra have been normalized to equal background intensity. Our spin-averaged data agree quantitatively with the spectra published earlier by Ortega *et al* [49]. A coverage of one or two monolayers of Co on Cu(100) seems to be sufficient to measure the first QW state 2 eV above the Fermi level. It is also clearly seen from figure 7(a) that, with increasing Co coverage, this peak slowly shifts to higher energies. At about 4 ML of Co a second QW state emerges. The third one starts to appear at about 10 ML. For larger thicknesses the direct sp-band transition within the three-dimensional band structure is formed. More detailed information can be obtained from the spin-resolved data shown in figure 7(b). Here, the open circles represent the minority channel and the filled ones indicate the majority states. A considerable amount of exchange splitting is observable in the spectra from 2 ML on. This is consistent with the thickness dependence of the Curie temperature for thin Co films [50]. The exchange splittings of the first two QW states have been determined to $\Delta_{ex} \approx 0.1$ and 0.2 eV.

Instead of analysing the experimental data within the commonly used PAM [46], we choose again the one-step model of photoemission together with a generalized resonance criterion. The fully relativistic theory, which is based on layer-KKR multiple scattering techniques, takes into account quantitatively the complex geometric structure of Co monolayers on Cu. As a first approach for spectroscopic calculations we used bulk muffin-tin potentials for fcc Co and fcc Cu to simulate a semi-infinite Cu bulk with 1 ML Co deposited on the Cu(100) surface. The interlayer distance of the Co monolayer has been chosen according to [51].

In figure 8, we present the spin-resolved spectral densities calculated for the $\bar{\Gamma}\bar{X}$ direction of the surface Brillouin zone. In both panels the grey shaded areas (vertical lines) represent the gap in the projected bulk band structure of Cu. The majority and minority gaps appearing in the projected bulk band structure of fcc Co have been shown by green and red shaded areas (horizontal lines). The energetic position of the corresponding $X_{4'}$ symmetry point for Co is 2.0 eV for majority spin electrons and 2.3 eV for minority states, respectively. Co surface bands are indicated by SB_{sp}. In addition to the expected QW state QW_{sp} a crystal-induced surface state SS_{sp} appears in the minority gap. Surprisingly, this feature is not found in the corresponding majority part. The situation becomes clearer when using the resonance condition (equation (14)) not only for electron confinement at the vacuum/Co interface (a) but also within the Co layer (b). From this analysis it turns out that the majority feature denoted by QW_{sp} possesses a considerable amount of spectral density in both regions (a) and (b). About 40% of the total density is located in region (a) and the remaining part in region (b). In the minority channel, two features are clearly separated in energy. Again the amount located in

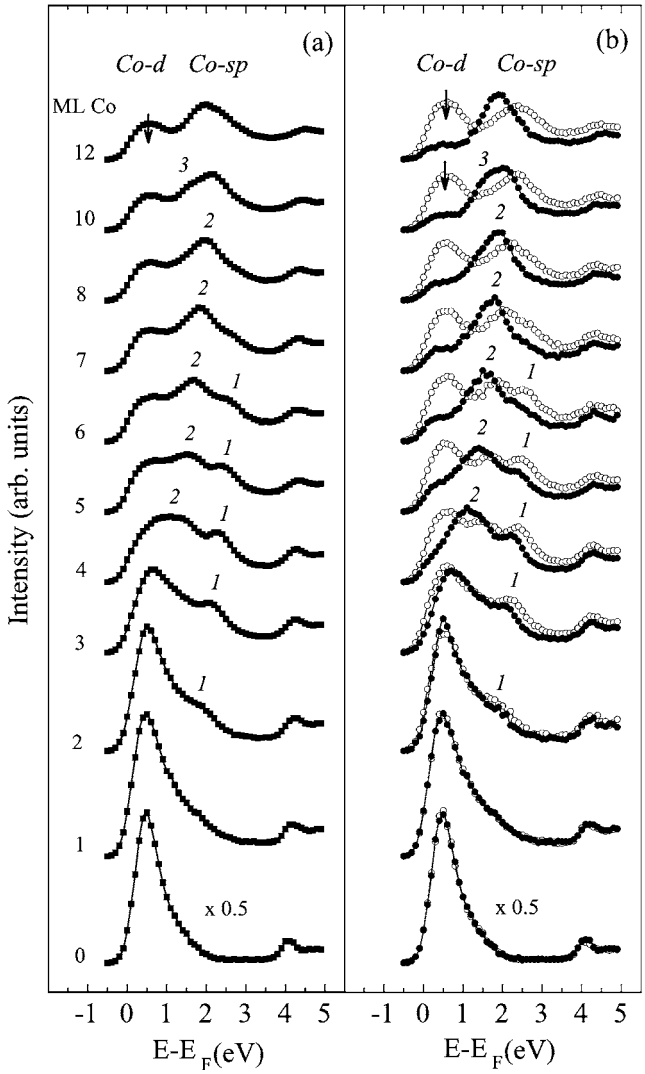

Figure 7. IPE spectra as a function of the Co coverage on Cu(100) for Co films up to 12 ML. The Cu spectra have been multiplied by a factor of 0.5. (a) Spin-averaged spectra; (b) spin-resolved data with open and filled circles denoting minority and majority spectra, respectively.

regions (a) and (b) has been determined by the resonance criterion. It turned out that the feature at higher energy is predominantly located in region (a), and therefore identified as surface state SS_{sp} (not yet identified experimentally), whereas the feature at lower energy definitely has QW character. As it should be, the QW state still disperses inside the region of confinement given by the difference in energy of the gap boundaries between Cu and Co. The calculated exchange splitting of QW_{sp} at $\bar{\Gamma}$ amounts to 200 meV, in line with the spin-resolved IPE data.

One may speculate about some tendency in the development of additional surface states. The clearcut separation in the minority channel between surface and QW states may result from the influence of the minority d bands, which are closer in energy by about 1 eV compared with the majority case. In the majority channel, however, the observed feature combines both

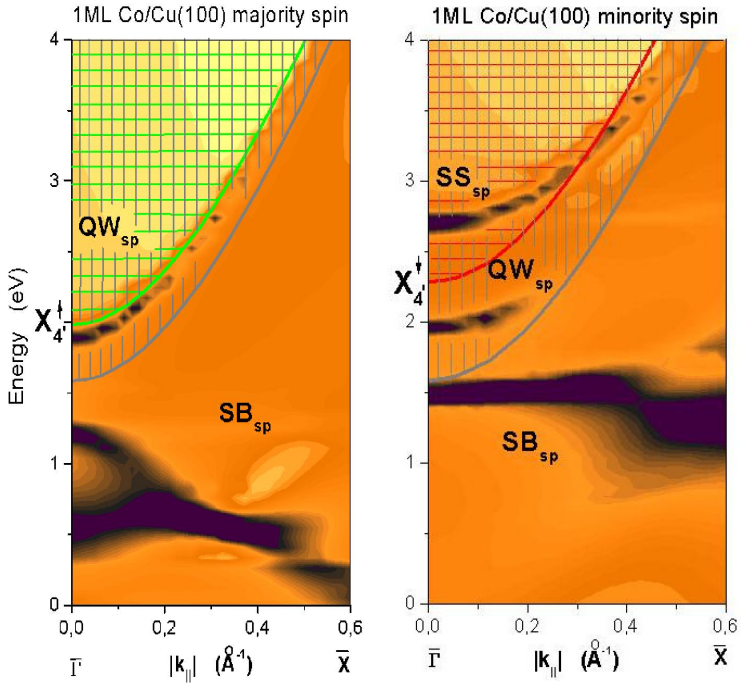

Figure 8. Contour plot for majority (left panel) and minority (right panel) (I)PE spectral densities of 1 ML Co/Cu(100) along $\bar{\Gamma}\bar{X}$. In both panels the grey shaded areas (vertical lines) represent the gap in the projected bulk band structure of Cu. The majority and minority gaps appearing in the projected bulk band structure of ferromagnetic fcc Co have been shown by green and red shaded areas (horizontal lines). Also the corresponding $X_{4'}^{\uparrow\downarrow}$ symmetry point is shown. SB_{sp} denotes Co surface bands. Surface state emission is indicated by the symbol SS_{sp}. QW_{sp} belongs to the first QW state.

surface and QW character. In conclusion, this analysis clearly shows that surface states and QW states can be described within the same theoretical approach. Further and more detailed studies along these lines are in progress.

6. Summary

The surface and interface electronic structure of simple metal surfaces and more complex systems like Co/Cu(100) have been determined by a detailed theoretical analysis of spin-resolved (I)PE data within the one-step model in combination with a generalized resonance criterion. Starting with Cu(111) we studied systematically the varying d-band influences on the surface electronic structure. A contest between surface resonances and surfaces states arises whose outcome is determined by the influence of d states. Surface resonances dominate with increasing d-band influence. On the basis of our results, most of the conflicting experimental data concerning Ni(111), Co(0001) and Fe(110) could be explained. Furthermore, the data obtained for Co/Cu(100) demonstrate that QW states, even in magnetic systems, may be understood along the same lines as the other surface features. Extrapolating to the near future, a microscopic understanding of the variety of surface and interface states in more complex magnetic multilayers has to be expected.

References

[1] Feuerbacher B, Fitton B and Willis R F (ed) 1978 *Photoemission and the Electronic Properties of Surfaces* (New York: Wiley)
Cardona M and Ley L (ed) 1978 *Photoemission in Solids* vol 1 (Berlin: Springer)
Inglesfield J E 1982 *Rep. Prog. Phys.* **45** 223
Courths R and Hüfner S 1984 *Phys. Rep.* **112** 53
Kevan S D (ed) 1992 Angle-resolved photoemission, theory and current applications *Studies in Surface Science and Catalysis* vol 74 (Amsterdam: Elsevier)

[2] Dose V 1983 *Prog. Surf. Sci.* **13** 225
Dose V 1985 *Surf. Sci. Rep.* **5** 337
Borstel G and Thörner G 1988 *Surf. Sci. Rep.* **8** 1
Smith N V 1988 *Rep. Prog. Phys.* **51** 1227
Donath M 1994 *Surf. Sci. Rep.* **20** 251

[3] Hohenberg P and Kohn W 1964 *Phys. Rev.* **136** 864
Kohn W and Sham L J 1965 *Phys. Rev.* **140** 1133
Sham L J and Kohn W 1966 *Phys. Rev.* **145** 561

[4] Jones R O and Gunnarsson O 1989 *Rev. Mod. Phys.* **61** 689

[5] Pendry J B 1974 *Low Energy Electron Diffraction* (London: Academic)

[6] Pendry J B 1976 *Surf. Sci.* **57** 679

[7] Hopkinson J F L, Pendry J B and Titterington D J 1980 *Comput. Phys. Commun.* **19** 69

[8] Ginatempo B, Durham P J and Gyorffy B I 1983 *J. Phys. C: Solid State Phys.* **1** 6483
Thörner G and Borstel G 1984 *Phys. Status Solidi* b **126** 617
Braun J, Thörner G and Borstel G 1985 *Phys. Status Solidi* b **130** 643
Braun J, Thörner G and Borstel G 1987 *Phys. Status Solidi* b **144** 609
Halilov S V, Tamura E, Gollisch H, Meinert D and Feder R 1993 *J. Phys.: Condens. Matter* **5** 3859
Henk J, Halilov S V, Scheunemann T and Feder R 1994 *Phys. Rev.* B **50** 8130
Fluchtmann M, Graß M, Braun J and Borstel G 1995 *Phys. Rev.* B **95** 9564

[9] Braun J 1996 *Rep. Prog. Phys.* **59** 1267

[10] Braun J 2001 New developments in UPS and XPS from ferromagnetic materials *Band-Ferromagnetism: Ground-State and Finite-Temperature Phenomena* ed K Baberschke, M Donath and W Nolting (Berlin: Springer) p 267

[11] Berglund C N and Spicer W E 1964 *Phys. Rev.* A **136** 1030

[12] Korringa J 1947 *Physica* **6/7** 392
Kohn W and Rostocker N 1954 *Phys. Rev.* **94** 1111
Kambe K 1967 *Z. Naturf.* a **22** 322
Williams A R and van Morgan J 1974 *J. Phys. C: Solid State Phys.* **7** 37
Brown R G and Ciftan M 1983 *Phys. Rev.* B **27** 4564
Zhang X-G, Gonis A and MacLaren J M 1989 *Phys. Rev.* B **40** 3694
Butler W H and Nesbet R K 1990 *Phys. Rev.* B **42** 1518
Ebert H and Gyorffy B L 1988 *J. Phys. F: Met. Phys.* **18** 451
Lovatt S C, Gyorffy B L and Guo G Y 1993 *J. Phys.: Condens. Matter* **5** 8005
Feder R 1981 *J. Phys. C: Solid State Phys.* **14** 2049

[13] Malmström G and Rundgren J 1980 *Comput. Phys. Commun.* **19** 263

[14] Pendry J B 1980 *Phys. Rev. Lett.* **45** 1381

[15] Borstel G 1985 *Appl. Phys.* A **38** 193

[16] Caroli C, Lederer-Rozenblatt D, Roulet B and Saint-James D 1973 *Phys. Rev.* B **8** 4552

[17] Hilgers G, Potthoff M, Müller N, Heinzmann U, Haunert L, Braun J and Borstel G 1995 *Phys. Rev.* B **52** 14859

[18] Rajagopal A K and Callaway J 1973 *Phys. Rev.* B **7** 1912

[19] Ramana M V and Rajagopal A K 1983 *Adv. Chem. Phys.* **54** 231

[20] Strange P, Ebert H and Gyorffy B L 1989 *J. Phys.: Condens. Matter* **1** 2959

[21] Calogero F 1967 *Variable Phase Approach to Potential Scattering* (New York: Academic)

[22] Ebert H and Gyorffy B L 1988 *J. Phys. F: Met. Phys.* **18** 451

[23] Gonis A 1992 Green functions for ordered and disordered systems *Studies in Mathematical Physics* vol 4 (Amsterdam: North-Holland)

[24] Wang X, Zhang X G, Butler W H, Stocks G M and Harmon B N 1992 *Phys. Rev.* B **46** 9352

[25] Lovatt S C, Gyorffy B L and Guo G Y 1993 *J. Phys.: Condens. Matter* **5** 8005

[26] Potthoff M, Lachnitt J, Nolting W and Braun J 1997 *Phys. Status Solidi* b **203** 441

[27] Grass M, Braun J, Borstel G, Schneider R, Dürr H, Fauster Th and Dose V 1993 *J. Phys.: Condens. Matter* **5** 599
[28] Echenique P M and Pendry J B 1978 *J. Phys. C: Solid State Phys.* **11** 2065
[29] McRae E G 1979 *Rev. Mod. Phys.* **51** 541
[30] Andersen O K 1975 *Phys. Rev.* B **12** 3060
[31] Math Ch, Braun J and Donath M 2001 *Surf. Sci.* **482–485** 556
[32] Kevan S D and Eberhardt W 1992 *Angle-Resolved Photoemission* ed S D Kevan (Amsterdam: Elsevier) p 99
Bertel E and Donath M (ed) 1995 *Electronic Surface and Interface States on Metallic Surfaces* (Singapore: World Scientific)
Borstel G and Inglesfield J E 2000 Electronic states on metal surfaces *Handbook of Surface Science* vol 2, ed K Horn and M Scheffler (Amsterdam: Elsevier) p 209
[33] Donath M 2001 Surface electronic structure of band ferromagnets *Band-Ferromagnetism: Ground-State and Finite-Temperature Phenomena* ed K Baberschke, M Donath and W Nolting (Berlin: Springer) p 267
[34] Donath M, Passek F and Dose V 1993 *Phys. Rev. Lett.* **70** 2802
[35] Braun J, Math Ch, Postnikov A and Donath M 2002 *Phys. Rev.* B **65** 184412
[36] Himpsel F J and Eastman D E 1978 *Phys. Rev. Lett.* **41** 507
[37] Borstel G, Thörner G, Donath M, Dose V and Goldmann A 1985 *Solid State Commun.* **55** 469
[38] Kutzner J, Paucksch R, Jabs C, Zacharias H and Braun J 1997 *Phys. Rev.* B **56** 16003
[39] Ishi S, Ohno Y and Viswanathan B 1985 *Surf. Sci.* **161** 349
[40] Himpsel F J and Eastman D E 1979 *Phys. Rev.* B **20** 3217
Himpsel F J and Eastman D E 1980 *Phys. Rev.* B **21** 3207
[41] Wetli E, Kreutz T J, Schmid H, Greber T, Osterwalder J and Hochstrasser M 1998 *Surf. Sci.* **402–404** 551
[42] Sakisaka Y, Rhodin Th and Mueller D 1985 *Solid State Commun.* **53** 793
[43] Vescovo E, Carbone C and Eberhardt W 1993 *Phys. Rev.* B **48** 285
[44] Kim H J, Vescovo E, Heinze S and Blügel S 2001 *Surf. Sci.* **478** 193
[45] Braun J and Donath M 2002 *Europhys. Lett.* **59** 592
[46] Smith N V, Brookes N B, Chang Y and Johnson P D 1994 *Phys. Rev.* B **49** 332
[47] Chiang T C 2000 *Surf. Sci. Rep.* **39** 181
[48] Yu D H, Donath M, Braun J and Rangelov G 2003 submitted
[49] Ortega J, Himpsel F J, Mankey G J and Willis R F 1993 *Phys. Rev.* B **47** 1540
[50] Schneider C M, Bressler P, Schuster P, Kirschner J, de Miguel J J and Miranda R 1990 *Phys. Rev. Lett.* **64** 1059
[51] Cerda J R, de Andres P L, Cebollada A, Miranda R, Navas E, Schuster P, Schneider C M and Kirschner J 1993 *J. Phys.: Condens. Matter* **5** 2055